Light Metals 2013

ALUMINUM ALLOYS: FABRICATION, CHARACTERIZATION AND APPLICATIONS

Casting and Solidification

SESSION CHAIR
Nagaumi Hiromi
Suzhou Research Institute
for Nonferrous Metals
Suzhou, China

ATOM PROBE ANALYSIS OF Sr DISTRIBUTION IN AlSi FOUNDRY ALLOYS

Jenifer Barrirero, Michael Engstler, Frank Mücklich

Functional Materials, Department of Materials Science, Saarland University, D-66123 Saarbrücken, Germany

Abstract

The addition of traces of Sr to AlSi foundry alloys induces a flake-to-fibrous transition of the eutectic phase which enhances tensile, impact and thermal shock properties. Since this modification is not always completely homogenous, the underlying mechanisms have to be reviewed. In this work the three dimensional Sr distribution in eutectic Si was analyzed by Laser Pulsed Atom Probe Tomography. Well modified fibers revealed nanometric segregations rich in Al and Sr. These features presented cluster-, planar- and rod-like morphologies which can be related to mechanisms involved in Si growth restriction. This finding reinforces the fact that Sr has a direct influence on the growth mechanism of eutectic Si.

Introduction

Al-Si alloys constitute the majority of Al castings. Si as the main alloying element imparts high fluidity, low shrinkage and a low thermal expansion coefficient, which results in good castability and weldability. Several industrial applications of these alloys are only possible due to the enhanced mechanical properties given by the chemical modification of the eutectic phase. The addition of trace elements, with Sr being the most commonly commercially used, causes a flake-to-fibrous transition which contributes to the improvement of tensile, impact and thermal shock properties [1]. The critical role in this modification is played by the Si phase where Sr is primarily segregated [2–5]. Three-dimensional analyses done by focused ion beam (FIB) tomography confirm the significant changes in the silicon morphology resulting from this modification [6].

Although several studies deal with the underlying mechanisms governing the solidification process of these modified alloys, it is still not possible to completely elucidate the influence of Sr on the change in microstructure. Some of the most accepted theories claim a Si growth restriction through the adsorption of the modifier element in the solid-liquid growth front. Lu and Hellawell [3] for instance, presented the impurity induced twinning (IIT) theory, through which step sources in Si would be poisoned by the modifier, promoting frequent twinning. Similarly, other authors [7–9] based their explanations on a mechanism which is believed to be operative in both, flake and fibrous eutectic: the twin plane re-entrant edge (TPRE) mechanism. In this case, the modifier will poison re-entrant {111} twin grooves. Shamsuzzoha and Hogan [10] used these ideas to propose a zigzag type of growth in which the branching mechanism induced by the modifier would be repeated indefinitely. Although slightly different, all these approaches are based on the hypothesis that, even if the morphology of eutectic Si appears to be almost isotropic, we are dealing with an anisotropic growth with high multiplication of changes in direction. Still, some researchers showed exceptions where no high density of twins could be detected [11,12]. Consequently, complementary mechanisms as,

for instance, nucleation mode and frequency [13–15], have also been proposed to play an important role.

In order to obtain a better understanding of the processes occurring during modification, a deep analysis of the modifier element distribution is essential. However, low Sr concentrations used for this purpose (commonly between 50 and 400 ppm) are below the detection limit of several spatially resolved chemical characterization methods such as energy or wavelength dispersive x-ray spectroscopy (EDS, WDS). Nogita *et al* [4] utilized an X-ray fluorescence microscope technique (μ-XRF) with sub-100 nm spatial resolution to show that Sr is relatively homogeneously distributed throughout the Si fibres. Moreover, Simensen *et al* [5], used secondary ion mass spectroscopy (NanoSIMS™) with lateral resolution down to 40 nm to analyse Na-modified alloys. Even though these methods had sufficient sensitivity to provide insight into Al-Si alloys, they could not yield strong evidence about the mechanisms involved. Recently, Timpel *et al* [16] employed Atom Probe Tomography (APT) and Transmission Electron Microscopy (TEM) to analyze Sr distribution in a Al-10 wt.% Si alloy. Evidence of inhomogeneous distribution of the modifier was presented, together with the proposal of two types of Sr-Al-Si co-segregations. Considering the fact that Atom Probe is an adequate technique to obtain chemical information up to the atomic scale, but that the volume size of the samples measured are extremely small, further analysis are needed in order to find more evidence on the mechanisms under discussion. Within the present study, Sr distribution in eutectic Si was further measured and analyzed by Laser Pulsed Atom Probe Tomography.

Materials and Experimental Procedures

High purity samples of nominal composition Al-7 wt% Si were used for this research. The production process was done by directional solidification in a Bridgman furnace with cooling rates of 0.25 K/s and 6.25 K/s. Al and Si, having both 99.99 wt% purity with Fe as the major impurity, were melted at the corresponding proportions. Sr was added at a nominal level of 150 ppm using an Al-10 wt.% Sr master alloy rod. Unmodified samples were used as reference.

A cross-sectional cut was first mechanically polished and further prepared in a dual-beam FIB (Helios NanoLab 600™, FEI Company). Site-specific sample preparation for atom probe tomography (APT) was done by the lift-out technique [17]. An electron beam induced Pt-cap layer was first deposited on the eutectic area in order to provide protection from gallium implantation. Afterwards, an isosceles shaped wedge was cut out (Fig.1 (a)) and transferred by means of an in-situ micromanipulator (Omniprobe AutoProbe™100) to a prefabricated Microtip™ array (CAMECA). The wedge was used to prepare several samples, which were welded and cut onto consecutive posts (Fig.1 (b)). An annular milling process was then performed in order to obtain specimens with an apex diameter

under 50 nm (Fig.1 (c)). The last preparation step was a low kV milling at 2 kV, a so called *clean up,* to reduce Ga implantation as much as possible.
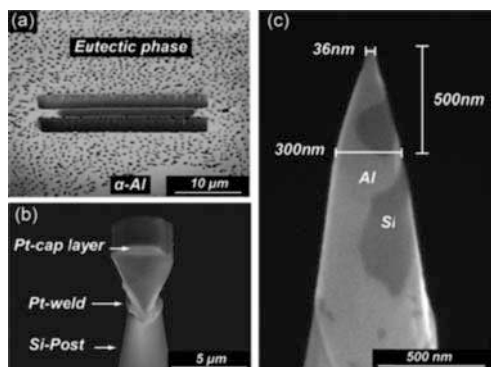

Fig.1: Site-specific sample preparation: Lift-out technique. (a) Triangular shaped wedge before lift-out; (b) Welded wedge; (c) Final specimen shape.

Laser Pulsed Atom Probe Tomography was carried out with a LEAP™ 3000X HR (CAMECA) at a pulse frequency of 250 kHz, a specimen temperature of 40 K and pressure lower than 1×10^{-10} Torr (1.33×10^{-8} Pa). The laser pulse energy was set between 0.2 and 0.6 nJ for Si specimens, while samples with an increasing amount of Al needed slightly higher energies. The target evaporation rate was of 5 atoms per 1000 pulses. Datasets were then reconstructed and analyzed with IVAS™3.6 software (CAMECA). Chemical analyses were carried out using iso-concentration and iso-density surfaces (voxel size = $0.5 \times 0.5 \times 0.5$ nm^3, delocalization distance = 3nm), proximity histograms, 1D concentration profiles and cumulative profiles.

Results

Optical micrographs of the alloys used within this study are presented in Fig.2. Primary α-Al dendrites are surrounded by plate-like eutectic phase in the case of the unmodified alloy; while modified eutectic shows coralline-like morphology. The distribution of Sr in the Si eutectic phase was studied in order to find confirming or denying proves of some of the hypotheses proposed in literature. Sr was only found in the Si phase and always segregated together with Al. Its distribution is markedly inhomogeneous with rod-, planar- and cluster-like segregations. Fig. 3, 4 and 5 show some examples of the solute-enriched features found.

Five rod-like segregations comparable to the one seen in Fig.3 were analyzed. Their diameters ranged between 2 - 4 nm with a length between 20 - 30 nm, although always limited by the confined measured volume. Because of their small size and bad statistics, it was not possible to use iso-concentration surfaces or proximity histograms to assess their concentrations. Compositional profiles were use qualitatively to evaluate the approximate spatial distribution of Al with respect to Sr (Fig.3). Average concentrations ranged between 1 - 3.4 at.% Al and 0.4 - 1.5 at.% Sr. The calculated Al:Sr ratio was between 2 to 3 for all rod-like segregations. The concentration measured outside the segregations were always below 0.01 at.% for both elements.
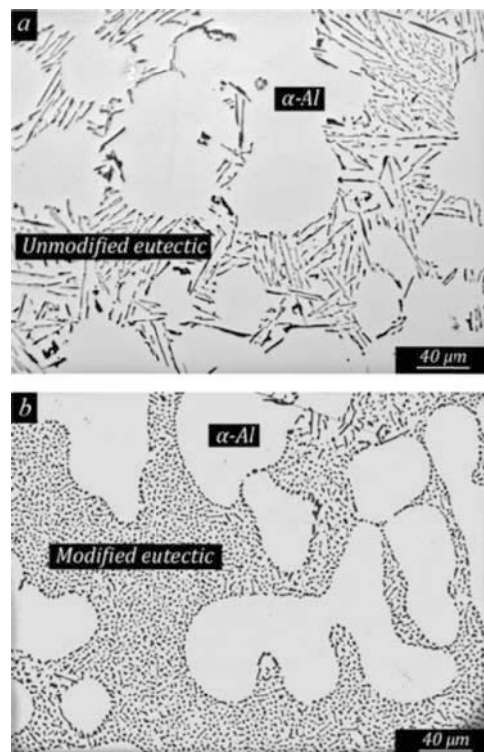

Fig.2: Optical micrograph of the Al 7wt.% Si alloy used for this study. (a) Unmodified alloy showing plate-like eutectic morphology; (b) Sr-modified alloy (150ppm) showing coralline-like morphology.

Fig.4 presents a plane-like segregation which is situated where Si changes its growth direction (Fig.4 (b)). Moreover, the iso-density surfaces (Fig.4 (a)) denote features comparable to those presented previously (rod-like). The spatial correlation between Al and Sr was evaluated by plotting the cumulative increase of these two elements with respect to the total
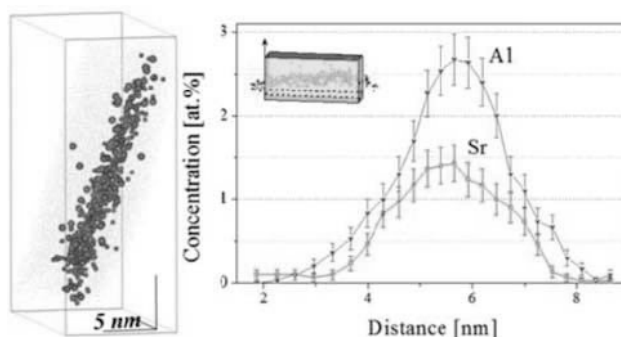

Fig.3: Region of interest (ROI) of an atom probe measurement showing a rod-like Al-Sr rich segregations in Si (green spheres represent Al and red spheres Sr). Concentration profile shows spatial distribution and ratio between Al and Sr.
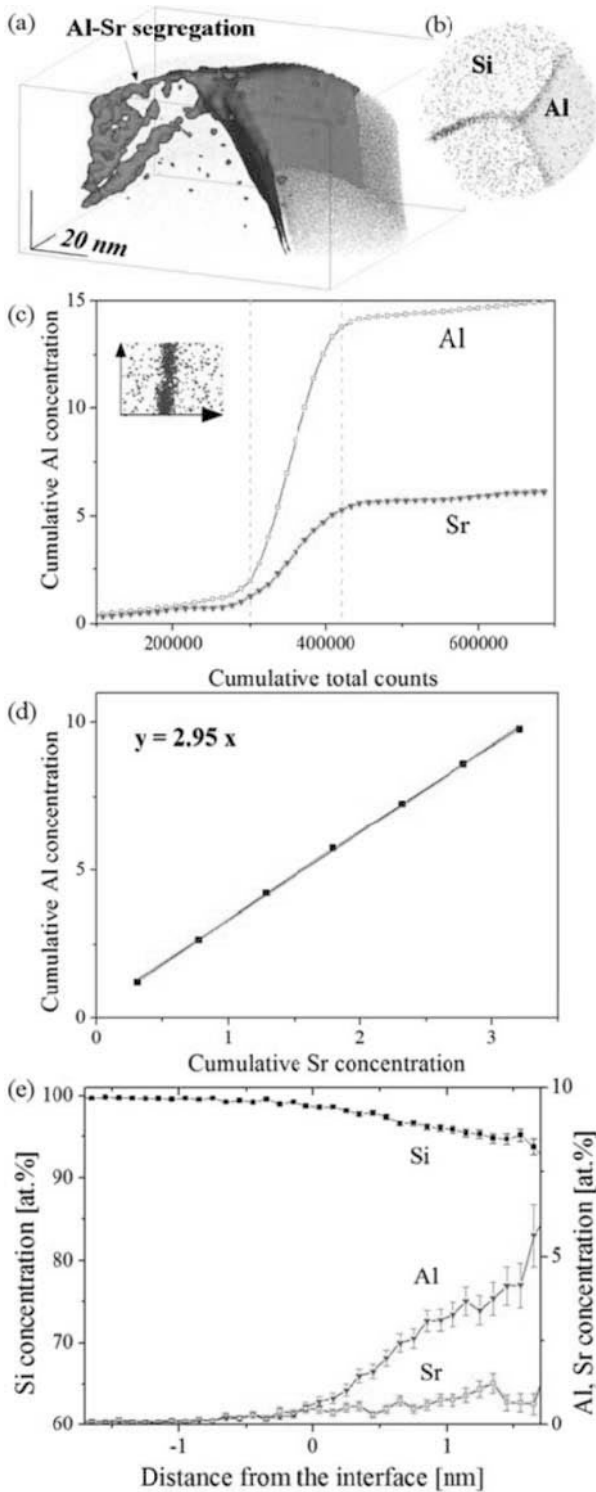
292

number of atoms (Fig.4 (c)). The concentration of both elements present a clear coincident change in slope (dashed lines) which indicates a concentration increment. This plot was also used to estimate the width of the segregation which was of 4 nm. To calculate the Al:Sr ratio, a ladder diagram was plotted (Fig.4 (d)). A linear correlation between Al and Sr was found and the Al:Sr ratio was of 2.95 as indicated by the slope. Finally, the concentration of this segregation was estimated by a proximity histogram which gives an in-depth compositional analysis (Fig.4 (e)) [18,19]. The cero point corresponds in this case to a iso-concentration surface with 1.1 at.% Al, and the positive and negative distances from the interface show the concentration inside and outside the segregation, respectively. The average concentration was calculated as the mean value between -0.85 to 1.65 nm in the proximity histogram. The concentration was found to be 1.9 at.% Al and 0.5 at.% Sr with an Al:Sr ratio of 3.8, somewhat higher than the previously calculated ratio.

Fig.4: Al-Si boundary in the eutectic phase: (a) Planar-like Al-Sr segregation (Iso-density surfaces: 0.25(#/nm^3) Al, 0.05 (#/nm^3) Sr); (b) Top view showing Si change in growth direction; (c) Cumulative diagram showing coincident change in slope for the segregating elements; (d) Ladder diagram showing a linear compositional correspondence between Al and Sr; (e) Proximity histogram from a 1.1 at.% Al iso-concentration surface.
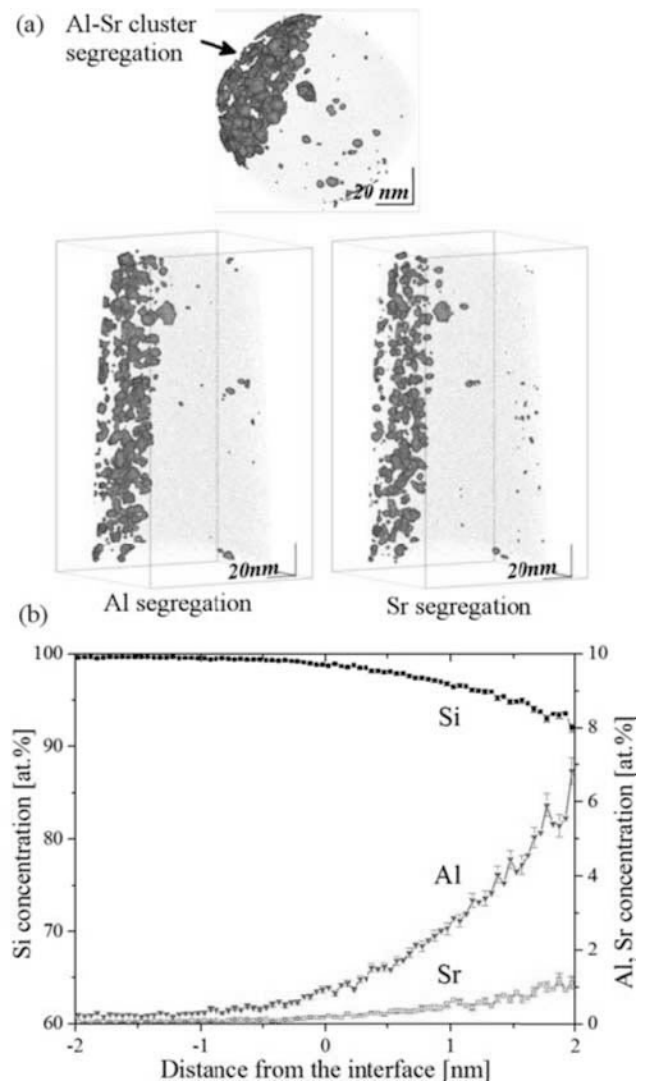
Fig.5: (a) Atom probe reconstruction showing a Si tip with cluster-like Al-Sr segregations (Iso-concentration surfaces: 2.4 at.% Al; 0.6 at.% Sr); (b) Proximity histogram from a 1.2 at.% Al iso-concentration surface.

A third type of segregations with approximately rounded form and a size ranging between approximately 5 and 15nm was found in a eutectic Si tip (Fig.5 (a)). This clustering is only present in one side of the tip and it is separated from the cluster-free zone by a planar limit. Al clusters showed a higher acquisition density (lower evaporation field) as compared with the Si matrix. This effect was taken into account while analyzing the data and a density correction algorithm available in the analysis software was applied. In order to evaluate the composition of the clusters, seven clusters with an iso-concentration surface of 1.2 at.% Al were used to create a proximity histogram (Fig.5 (b)). The concentration of these clusters was calculated by averaging from -1 to 1.8 nm and it was found to be 1.9 at.% Al, 0.4 at.%Sr, showing an Al:Sr ratio of 4.75.
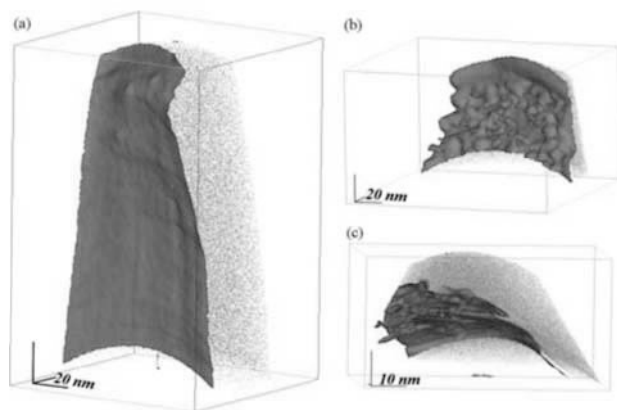

Fig.6: Al-Si boundary morphology. (a) Sr-modified alloy with smooth Al-Si interface (Iso-concentration surface: 20 at.% Al); (b,c) Unmodified alloy with irregular jagged Al-Si boundary (Iso-concentration surface: 4 at.% and 20 at.% Al, respectively).

The concentration of Sr at the Al-Si boundary was analyzed by the use of proximity histograms and concentration profiles, but no significant segregation of Sr was detected. However, some inconveniences which challenged this analysis should be mentioned. Firstly, gallium introduced during focused ion beam sample preparation is preferentially implanted into the Al-Si boundary. Secondly, higher random background noise and higher amount of hydrogen was detected in the Si phase. Although a background subtraction methodology was applied for the analysis, concentrations lower than 0.2 at.% could not be analyzed in Si due to this effect. On top of that, a comparative analysis between the Al-Si boundary morphologies of unmodified and Sr-modified samples was done. The morphological evolution of the interfaces was evaluated by iso-concentration surfaces of Al and Si through a wide range of concentrations. Fig.6 shows Al iso-concentration surfaces as one example of this comparison. Unmodified samples presented an inhomogeneous jagged boundary while Sr-modified samples showed a smoother boundary.

Discussion

The evidence found within this investigation helps to bring light to the operative mechanisms of the Sr-modification of AlSi hypoeutectic alloys. The presence of rod-like and planar-like segregations are in accordance with the hypotheses of a restriction in Si growth proposed during the 70s and 80s [3,7–9,20], and confirms the recently published results of Timpel et al. [16]. However, although the most basic hypothesis of growth restriction is supported, plenty of new questions arise. Why Al is always segregated together with Sr? In what extend is Si present in these segregations? Are we in presence of nanometric intermetallic phases? Which is the role of the rounded clusters?

Theories as for example the impurity induced twinning (IIT) [3], suggested only the presence of Sr without suspecting that Al is also there. IIT theory proposed that a preferential absorption of modifying elements into the Si liquid front would promote a change in the silicon {111} stacking sequence, and thereby, increase the twinning frequency by creating "traffic problems". They suggested an optimal *hard sphere radius ratio* of $r_{modifier}:r_{Si} \approx 1.65$ which would force the growing step to miss one regular close packed position, fall into the next stacking sequence, and give rise to a twin. This geometrical model is approximately in agreement, for instance, with Sr ($r_{Sr}:r_{Si}=1.84$) or Na ($r_{Na}:r_{Si}=1.59$) as pure elements poisoning Si. However, since in the present work segregations contain two to three times more Al than Sr, this assumption would not be confirmed. Al has a considerably lower radius ratio than the theoretical value ($r_{Al}:r_{Si}=1.22$). Furthermore, the approximate width calculated for the segregations (2 to 4 nm) denote that several layers of atoms are involved, what also disagrees with the proposed size relation. These discrepancies indicate that the size factor proposed is not the principal requirement for the modification to occur. In this regard, the suggestion of the removal of growth advantage of the TPRE mechanism by concentration of the modifier at the re-entrant edges [7,8] is more accurate. The segregations found in this study can be in accordance with this hypothesis. The rod-like segregation would increase the incidence of branching, and consequently, minimize the anisotropic growth habit of Si. Moreover, the finding of a planar segregation agrees with the "Zigzag" type of growth proposed by Shamsuzzoha [10], who stated that the modifying impurity would be adsorb on {111} silicon surfaces and lower the {111} twin boundary energy.

The presence of clusters was not proposed by any of these theories. Timpel et al. [16] showed an EDX mapping of modified Si which showed Al clusters. Only some of these clusters had coincident Sr content. In the atom probe analysis done in the present study, Sr had a very good spatial correlation with Al (Fig.5 (a)) and no pure Al segregations were seen. This result could be related to a better chemical resolution of atom probe with respect to EDX. Two possible interpretations of these features can be done: they could be agglomerations due to excess of Sr in the alloy, or they could also restrict the growth of eutectic Si. Fig.5 shows that almost all segregations are situated behind a "virtual" plane, which is approximately parallel to the atom probe measurement. This direction is also coincident with the directional solidification axis. It can be thought as if Si has grown without restriction in the right-hand side of the sample, while the agglomerates in the left-hand side have stopped or forced a change in direction of the Si growth. Such wide areas with high density of segregations can explain a massive change of direction growth resulting in the formation of a coralline-like morphology. If not only rod-like, or planar-like segregations, but also rounded agglomerations induce changes in directions, this would better explain the activation of several twinning planes.

The fact that clusters have higher Al:Sr ratio than the other type of segregations, lead us to believe that they have a different origin.

One possible explanation could be the formation of pre-eutectic nanometric phases, or nanometric residual Al-Sr intermetallics of the Al-Sr Master alloy used for the manufacturing process. It should be emphasized that in no case, pure Sr segregations were found in the eutectic Si phase.

The challenge now is to try to find the stoichiometry of Si in these segregations. Timpel et al. [16] proposed intermetallic phases of $SrAl_2Si_{88}$ and $SrAl_4Si_{33}$ stoichiometry. These compositions does not fit exactly with the here presented results. Moreover, experimental artifacts inherent to the technique should be taken into account. One of these effects is a potential ion deflection arising from trajectory aberrations. The difference of field of evaporation needed by Al and Si to be detached influences the distribution of the electric field in the vicinity of the specimen's surface. This localized variations induce undesirable lateral displacement of ions during the first instant of their flight. In this particular case, the presence of a low-field evaporation precipitate (Al) will result in a lower field region that deflects the ion trajectories inwards because of a flattening of the surface at this point [21]. If we think now, that Al and perhaps some surrounding Si atoms could suffer from this deflection, we may have some difficulties in defining the real limit of the enriched zone. Besides, as the size or thickness of these features gets smaller, this aberration leads to higher uncertainty in composition. The distribution and concentration of Si (as the matrix element) inside of the solute-enriched features cannot be easily established. This is also the reason why, along this study we refer to Al-Sr enriched features without making reference to the amount of Si.

The addition of trace elements not only causes a flake-to-fibrous transition and a eutectic Si refinement, but also increases undercooling of the eutectic arrest. This effect is believed to be the consequence of a change in the growth mechanism. During solidification, Si flakes project ahead of the Al phase. Al is then forced to re-nucleate repeatedly between Si in order to maintain an approximately equal growth rate of the two eutectic phases [7]. This is the reason why Al in the eutectic phase of unmodified alloys is polycrystalline and the interface between Al and Si shows an irregular morphology (Fig.6 (b,c)). On the other hand, modified alloys do not show Si growth advantage. In contrast, both phases grow co-operatively at a common solid-liquid interface [7]. Al presents larger elongated grains without epitaxial relation to Si. The homogeneous smooth interface profile found in the Sr-modified alloy (Fig.6 (a)) proves this suppression of Si leading distance.

One of the mechanisms proposed by Kobayashi and Hogan [7] which could account for this change in growth mechanism, was a change in interfacial-energies due to the accumulation of the modifying element at the boundary. However, this hypothesis was not confirmed by the experimental results obtained during this study. An alternative explanation which better fits our results is that Al-Sr segregations restrict Si growth causing a great increase of changes in growth direction. These changes in direction increase the growth flexibility and the TPRE anisotropic advantage is sufficiently reduced to result in a strongly coupled growth with a smooth interface profile.

Conclusion

The present study shows that atom probe tomography is an adequate characterization method for the study of Al-Si alloys.

Nanometric segregations rich in Al and Sr were found in eutectic silicon. These features having rod-, planar- and cluster-like morphologies are in accordance with theories proposing Si growth restriction. On top of that, the loss of Si growth advantage during solidification of modified alloys was also confirmed. The presence of Al within the segregations, however, was not expected by the postulated theories, opening a new path towards the investigation of modified Al-Si alloys.

References

1. John E. Gruzleski, and Bernard Closset, *Treatment of Liquid Aluminum-Silicon Alloys* (Amer Foundrymens Society, 1990).

2. L. Clapham, and R. Smith, "Segregation behaviour of strontium in modified and unmodified Al-Si alloys," *Journal of Crystal Growth*, 92 (1988), 263–270.

3. S. Lu, and A. Hellawell, "The mechanism of silicon modification in aluminum-silicon alloys: impurity induced twinning," *Metallurgical and Materials Transactions A*, 18 (1987), 1721–1733.

4. K. Nogita et al., "Determination of strontium segregation in modified hypoeutectic Al–Si alloy by micro X-ray fluorescence analysis," *Scripta Materialia*, 55 (2006), 787–790.

5. C.J. Simensen et al., "NanoSIMS Analysis of Trace Element Segregation during the Al-Si Eutectic Reaction," *Metallurgical and Materials Transactions A*, 38 (2007), 1448–1451.

6. F. Lasagni et al., "Three Dimensional Characterization of Unmodified and Sr-Modified Al-Si Eutectics by FIB and FIB EDX Tomography," *Advanced Engineering Materials*, 8 (2006), 719–723.

7. K. Kobayashi, and L. Hogan, "The crystal growth of silicon in Al-Si alloys," *Journal of Materials Science*, 20 (1985), 1961–1975.

8. M.G. Day, and A. Hellawell, "The Microstructure and Crystallography of Aluminium-Silicon Eutectic Alloys," *Proceedings of the Royal Society A: Mathematical, Physical and Engineering Sciences*, 305 (1968), 473–491.

9. M. Shamsuzzoha, and L.M. Hogan, "The twinned growth of silicon in chill-modified Al–Si eutectic," *Journal of Crystal Growth*, 82 (1987), 598–610.

10. M. Shamsuzzoha, and L.M. Hogan, "The crystal morphology of fibrous silicon in strontium-modified Al-Si eutectic," *Philosophical Magazine A*, 54 (1986), 459–477.

11. J. Chang, and H. Ko, "Twin probability of eutectic Si in rare earth modified Al-7wt% Si alloy," *Journal of Materials Science Letters*, 19 (2000), 197–199.

12. K. Nogita, J. Drennan, and A. Dahle, "Evaluation of silicon twinning in hypo-eutectic Al-Si alloys," *Materials Transactions*, 44 (2003), 625–628.

13. Y.H. Cho et al., "Effect of Strontium and Phosphorus on Eutectic Al-Si Nucleation and Formation of β-Al5FeSi in Hypoeutectic Al-Si Foundry Alloys," *Metallurgical and Materials Transactions A*, 39 (2008), 2435–2448.

14. A.K. Dahle et al., "Eutectic nucleation and growth in hypoeutectic Al-Si alloys at different strontium levels," *Metallurgical and Materials Transactions A*, 32 (2001), 949–960.

15. S.D. McDonald et al., "Eutectic grains in unmodified and strontium-modified hypoeutectic aluminum-silicon alloys," *Metallurgical and Materials Transactions A*, 35 (2004), 1829–1837.

16. M. Timpel et al., "The role of strontium in modifying aluminium–silicon alloys," *Acta Materialia*, 60 (2012), 3920–3928.

17. K. Thompson et al., "In situ site-specific specimen preparation for atom probe tomography.," *Ultramicroscopy*, 107 (2007), 131–9.

18. O. Hellman et al., "Analysis of Three-dimensional Atom-probe Data by the Proximity Histogram.," *Microscopy and Microanalysis: the Official Journal of Microscopy Society of America, Microbeam Analysis Society, Microscopical Society of Canada*, 6 (2000), 437–444.

19. O.C. Hellman, J.B. du Rivage, and D.N. Seidman, "Efficient sampling for three-dimensional atom probe microscopy data.," *Ultramicroscopy*, 95 (2003), 199–205.

20. M.D. Hanna, S.-Z. Lu, and A. Hellawell, "Modification in the aluminum silicon system," *Metallurgical Transactions A*, 15 (1984), 459–469.

21. B. Gault et al., *Atom Probe Microscopy* (Springer New York, New York, NY, 2012)185:188.